HHS Public Access

Author manuscript

Macromol Mater Eng. Author manuscript; available in PMC 2023 October 01.

Published in final edited form as:

Macromol Mater Eng. 2022 October ; 307(10): . doi:10.1002/mame.202200196.

Extracellular Matrix Microparticles Improve GelMA Bioink Resolution for 3D Bioprinting at Ambient Temperature

Zachary Galliger,
Biomedical Engineering Graduate Program, University of Minnesota, Minneapolis, MN.

Caleb D. Vogt,
Biomedical Engineering Graduate Program; Medical Scientist Training Program, University of Minnesota, 420 Delaware St. SE, Minneapolis, MN.

Haylie R. Helms,
Department of Pediatrics, Division of Blood and Marrow Transplantation & Cell Therapy, University of Minnesota, 420 Delaware St. SE, Minneapolis, MN.

Angela Panoskaltsis-Mortari*
Department of Pediatrics, Division of Blood and Marrow Transplantation & Cell Therapy; Department of Medicine, Division of Pulmonary, Allergy, Critical Care & Sleep, University of Minnesota, 420 Delaware St. SE., Minneapolis, MN.

Abstract

Introduction: Current bioinks for 3D bioprinting, such as gelatin-methacryloyl, are generally low viscosity fluids at room temperature, requiring specialized systems to create complex geometries.

Methods and Results: Adding decellularized extracellular matrix microparticles derived from porcine tracheal cartilage to gelatin-methacryloyl creates a yield stress fluid capable of forming self-supporting structures. This bioink blend performs similarly at 25°C to gelatin-methacryloyl alone at 15°C in linear resolution, print fidelity, and tensile mechanics.

Conclusion: This method lowers barriers to manufacturing complex tissue geometries and removes the need for cooling systems.

Graphical Abstract

*corresponding author: A. Panoskaltsis-Mortari, Department of Pediatrics, Division of Blood and Marrow Transplantation & Cell Therapy; Department of Medicine, Division of Pulmonary, Allergy, Critical Care & Sleep, University of Minnesota, 420 Delaware St. SE., Minneapolis, MN. panos001@umn.edu.

Ethics Statement & Conflict of Interest

Ethical approval of this work was not required. The authors declare no conflict of interest for this work.

AIP Publishing Data Sharing Policy

The data that support the findings of this study are available from the corresponding author upon reasonable request.

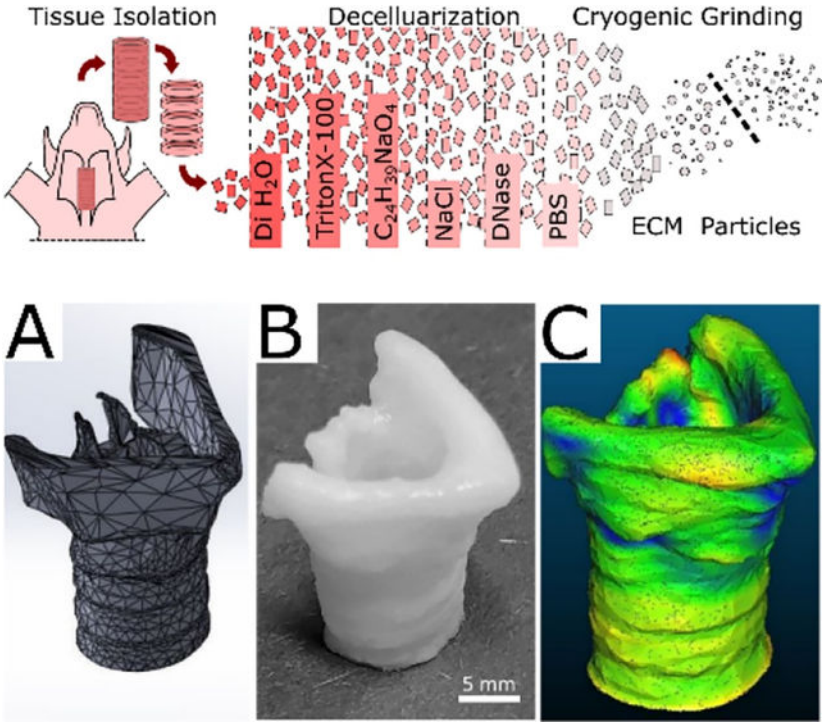

Decellularized extracellular matrix particles derived from porcine tracheal cartilage are added to gelatin-methacryloyl, creating a yield stress fluid capable of forming self-supporting structures. This bioink blend performs similarly at 25°C to gelatin methacryloyl alone at 15°C in linear resolution, print fidelity, and tensile mechanics. This removes the need for cooling systems to manufacture self-supporting complex tissue geometries.

Keywords

hydrogel; extracellular matrix; 3D bioprinting; tissue engineering; trachea; larynx

Introduction:

3D bioprinting has the potential for the rapid production of patient-specific, tissue-engineered constructs. The continued growth and versatility of bioprinting depends on the development of novel printable hydrogels, called bioinks, that provide mechanical support, cell adhesion sites, and promote the function of the printed tissue. Gelatin methacryloyl (GelMA) is a commonly used bioink because of its tunable mechanical and chemical properties, relatively low cost, and ability to be remodeled by mammalian cells.[1] GelMA relies on covalently crosslinking methacrylamide side groups, usually via a photoinitiator. These covalent bonds significantly increase its stiffness and stability compared to thermal gelation alone. Other proteins have been similarly modified to create photocrosslinkable hydrogels, such as collagen I to ColMA, or hyaluronic acid to HAMA.[2,3] Unfortunately, most of these materials have a narrow window of use; at room temperature they are unable to support themselves and fail to print complex structures without specialized methods. The field has managed this shortcoming by casting simple geometries, printing

at low temperatures, or printing into a sacrificial support bath.[4] While these methods widen the utility of these materials, they face many challenges in scaling the process to clinically relevant manufacturing. Furthermore, these bioinks alone do not fully capture the complexity of native extracellular matrix (ECM), thus limiting their ability to recapitulate native microenvironments.

Whole organ decellularization is the leading approach to capture both the organization and diversity of tissue structure.[5] Decellularized tracheal and laryngeal cartilage has even been shown to promote cartilage generation *in vivo*.[6–8] However, the approach is less effective for dense tissues and requires a donor tissue of a similar size to the target transplant or model. To overcome these limitations, decellularized ECM (dECM) could be processed into tissue-specific bioinks and 3D bioprinted into the required tissue matching the size and geometry required by the patient. This is significantly impactful for developing airway grafts for pediatric patients who have a limited donor pool and large variation in tissue size.

Most commonly, a soluble fraction of dECM is isolated using protein denaturation or enzymatic digestion, then added to a bioink solution to provide tissue specificity or binding sites.[9–19] Other methods modify the dECM with cross-linking groups to incorporate them covalently with the bioink, improving the mechanics of the construct but potentially decreasing the bioactive benefits of the ECM.[20,21] An alternative method is using decellularized tissue particles, which has shown beneficial chondrogenic effects in the literature and may minimize protein denaturation.[22,23]

The rheology of complex fluids such as cell-laden bioinks, is dependent on the size distribution of the particles, the interactions between these particles and the solvent, the interactions between the particles themselves, and the mechanics of the particles.[24] Generally, smaller particles and higher concentrations of particles lead to increased viscosity based on the collective surface area interacting with the bulk fluid.[25] Previous studies have shown that high density cell suspensions exhibit properties of Bingham plastics and have been used as a bioprinting medium.[26] Alternatively, this idea can be used to create a yield stress fluid bioink using high cell density or particle concentration.[22] We hypothesized that the addition of decellularized cartilage tissue particles to GelMA bioinks would widen the temperature range of GelMA 3D extrusion bioprinting, improving print resolution and fidelity.

Results:

Synthesis and Characterization of GelMA

During GelMA synthesis, methacryloyl groups are added to the primary amines of lysine and hydroxylysine in the gelatin.[27–29] Measuring the concentration of primary amines in GelMA compared to the unmodified gelatin using a TNBS assay, provides an estimate of the degree of primary amine modification. The GelMA used in this study was determined to be 94 ± 1% modified (Supplemental Figure 1A). The addition of methacryloyl groups was confirmed with the emergence of two peaks between 5 and 6 ppm in the H-NMR spectra (Supplemental Figure 1B). Using a temperature sweep, the gelation point of 5% wt/v GelMA was determined by modulus crossover to be 15.1 ± 0.1°C (Supplemental Figure 1C).

Decellularization and Particle Characterization

To verify the decellularization, the DNA content was measured using a fluorescence intensity assay. The dECM particles contained 1.2 ± 0.1 nanogram of DNA per milligram of dry tissue, less than 2% percent that of native tissue and well below the published decellularization threshold of 50 ng DNA per mg (Supplemental Figure 2A).[3] After cryomilling and filtering, the average particle radius was 29 ± 23 μm, and 75% of all particles were below 50 μm (Supplemental Figure 2B & C). Combining 10% dECM particles with 5% GelMA produced a bioink that did not exhibit a thermal gelation point between 10°C to 25°C (Supplemental Figure 2D).

Trichrome staining showed the preservation of fibrillar ECM proteins in the particle laden hydrogel and safranin-O staining indicated the glycosaminoglycans in the ECM as well (Supplemental Figure 3). Histology also revealed residual cellular components in the lacunae of the cartilage indicating that low DNA content should not be used as the sole means of determining removal of cellular material.

Dose Dependency of dECM particles on Rheology

To characterize the effect of adding dECM particles to GelMA, a range of concentrations were produced from 0 – 10% wt/v in a 5% wt/v GelMA solution. A parallel plate rheometer was used to characterize the fluid behavior at 25°C. A shear rate flow sweep demonstrated a concentration-dependent effect of the particles on the viscosity of the fluid. The 0% dECM 5% GelMA solution at 25°C was well above its gelation temperature of 15°C and thus behaved as a moderately shear thinning fluid with relatively low viscosity (Figure 1A). Addition of even 5% dECM significantly changed the behavior, increasing the low-shear viscosity and imparting a more pronounced shear thinning behavior. Increased amounts of particles yielded a predictably higher viscosity and maintained the shear-thinning property.

Oscillatory rheometry was used to characterize the shear stress response to ascending shear rate sweep (Figure 1B). As expected from the viscosity results, the generated shear stress increased with increasing particle concentrations. The results also indicated a possible change in yield stress at the start of flow, which was further investigated by stress-controlled oscillatory sweeps. Low amplitude oscillations demonstrated a dominant storage modulus (G') consistent with the linear viscoelastic region prior to fluid yield. As the stress increased, the storage modulus decreased, and the loss modulus became dominant. Yield stress was estimated by fitting the data to a Herschel-Bulkley model (95% confidence intervals for the model parameters are listed in Table 1). This was used rather than estimating the yield stress from the modulus crossover point because some samples either exhibited solid or liquid behavior throughout the stress range (Supplemental Figure 4). The particle suspensions showed an increasing apparent yield stress in a concentration-dependent manner (Figure 1C).

Print Resolution

The resolution of pressure-driven extrusion 3D bioprinting relies on the interplay of many factors. Some factors are a complex result of the rheological properties and the cross-linking rate specific to the bioink formulation and crosslinking mechanism. Others are easily

manipulated by changing the printer setup or machine code: tip diameter, printing speed, driving pressure, and stage height.[30] This creates a multi-parameter space, where varying any of the factors will change the print resolution. Blends of 5% wt/v GelMA with 0% to 10% wt/v dECM particles were tested from 25 kPa to 200 kPa using constant print speed (5 mm/s), and stage height (0.1 mm) through 20Ga, 22Ga, and 23Ga × ½" cylindrical tips (Figure 1 D–F). At 25°C, 5% GelMA was above its gelation point and unstable as a bioink. At 10% wt/v dECM, the linear resolution at 25°C was significantly lower than with 5% GelMA alone printed at 15°C, at pressures below 100kPa for 20Ga tip, 150kPa for 21Ga tip, and 200kPa for 22Ga tip (Supplemental Table 1). The 10% dECM, 25°C bioink also exhibited the highest resolution using the 23Ga tip with a line width of 250 ± 40 μm at 75kPa, compared to 5% dECM, 25°C with 470 ± 40 μm and GelMA alone at 15°C with 960 ± 30 μm.

Print Fidelity and Reproducibility

Beyond linear resolution, the bioink must be able to reproduce a 3D model with minimal deformation. With unstable bioinks, as layers are added they can collapse and flow rather than discretely stack, potentially losing key features of the intended geometry. The effects of the dECM were evaluated by comparing the fidelity and reproducibility of dECM-laden constructs to GelMA alone using the same g-code for a hollow tube 5 layers tall. Both reliably produced hollow cylindrical constructs (Figure 2A–B). The width of the wall of the dECM-laden wall was significantly thinner than the GelMA alone (Figure 2C), 540 ± 20 μm and 800 ± 10 μm respectively, leading to a significant difference in lumen area (Figure 2D). Construct height and circularity exhibited minimal differences (Figure 2E & F). The ring constructs were further compared using tensile testing (Figure 2F). The stress at failure remained similar for the GelMA with or without ECM, but the strain at failure significantly decreased from 74±2% to 51±1%. (Figure 2G & H).

To further explore the dECM bioink, more complex carina and larynx geometries were printed. A pediatric scale carina model was designed and printed using 10% dECM, 5% GelMA, 1% LAP and compared with just 5% GelMA and 1% LAP (Figure 3 A–F). While the dECM-laden bioink was printed easily at 25°C, the GelMA bioink by itself required a chilled syringe (15°C), chilled build plate (10°C), and continuous crosslinking. If the syringe warmed above 15°C, the GelMA bioink would become fully liquid and unprintable. Similarly, if the build plate were at room temperature the bioink would melt and pool before being able to crosslink. Further, if the construct were not continuously crosslinked, layers between the build plate and syringe would warm from contact with surrounding air and melt. Once these bioprinted constructs were completed, to measure their fidelity, a 3D surface was reconstructed from micro CT imaging and compared to the initial carina model (Figure 3 A–F). From visual inspection, the dECM better forms the model's height and branch angle compared to the GelMA alone. The distances between the carina model and reconstructed surface were calculated and plotted as a heat map (Figure 3 G&H). The average distance for dECM bioink was 0.5 ± 0.4 mm, with 97% of the bioprinted construct within 1.5 mm of the initial model. In contrast, average distance for the GelMA alone was 0.5 ± 0.5 mm, with 93% of the construct within 1.5 mm of the initial model (Figure 3 I).

The bioprinted larynx construct reached 21 mm in height, with a top flaring to 12×17 mm over the 8×12 mm diameter base. To measure the fidelity of the bioprinted construct, a 3D surface was reconstructed from micro-CT imaging and compared to the initial larynx model. The distances between the larynx model and reconstructed surface were calculated and plotted as a heat map (Figure 4). The average distance was 0.9 ± 0.4 mm. 95% of the bioprinted construct was within 1.5 mm of the initial model.

Discussion:

In this study, we demonstrate the stabilizing effect of decellularized ECM particles on GelMA bioprinting. Bioprinting with GelMA alone is a manufacturing challenge because of its sensitivity to temperature perturbations. If the bioink warms above its gel point at any time before the print is completed and crosslinked, it will greatly deform. The entire printing chamber could be cooled below the gel point, but that becomes a logistical challenge for scaling up and maintenance costs. The GelMA print can be continuously crosslinked, but this excessive exposure to intense light puts stress on the embedded cells and will likely decrease post-print viability. Another option would be to only crosslink during layer changes. Depending on the design of the bioprinter, this adds significant time to the printing process; between each layer, the print head and light source need to exchange places twice. Extended printing time negatively impacts attachment-dependent cell types in suspension in the bioink and allows for the GelMA in the tip to warm to room temperature during layer changes, causing greater print variability. The current leading approach to printing with low-density GelMA and other low viscosity bioinks is using a sacrificial support bath, such as the gelatin particle slurry used in the FRESH method.[31,32] In this approach, the low viscosity bioink is suspended in the bath before and after crosslinking, preventing deformation before the bioink has solidified. However, to embed the construct within the support bath, the extrusion needle needs to reach through the bath to the lowest layer of the print. For larger printed constructs this may pose an issue, since increasing needle length also impacts the required driving pressure for print speed and the shear forces cells may experience.

Alternatively, we have shown that adding dECM particles to GelMA allows for reliable bioprinting at room temperature, removing these challenges from the manufacturing process. This is likely due to both increases in viscosity and development of significant yield stress, which resist fluid flow and structural deformation after the bioink is printed. This yield stress, coupled with shear thinning behavior, indicates that the bioink may be best modeled as a Herschel-Bulkley type fluid.

In future work, we expect that cells will benefit from the shear thinning nature of the bioink, as such fluids help to decrease the shear stress experienced by the cells during flow in the printing process. Further, the addition of ECM particles may allow for tissue specificity and greater influence over cell behavior which may be clearer with higher cell seeding density. Our understanding of the role of ECM as an instructive substrate is constantly expanding. Prior work in the literature has shown that articular and elastic cartilage ECM promotes the differentiation of mesenchymal stromal cells (MSCs) to chondrocytes.[33–38] At this time, the specific ECM proteins and signaling pathways that facilitate this differentiation

are unknown. However, instructive proteoglycans that compose a small percent of the ECM have been implicated. [39,40] Using minimally processed ECM may better retain its bioactivity, producing more reliable cellular constructs. On an industrial scale, a top-down approach (processing porcine tissues to derive tissue specific ECM) may be more cost-effective than isolating or producing specific ECM components from various sources and recombining them.

Conclusion:

This work shows the utility of ECM-derived particles as a bioink additive from a rheological and print parameter perspective. These particles significantly improve the printability of GelMA bioinks at room temperature without requiring support or suspension gels for printing complex structures. This lowers the barriers to bioprinting complex tissue models and circumvents many manufacturing challenges. Continuing this work, the biological effects of these particles should be examined. Evaluating their ability to influence cells and mature into viable tissues will be key to developing more reliable tissue grafts and accurate disease models. It will also be of interest to examine the effects of ECM particles derived from other tissues, examining if these rheological aspects are unique to cartilage ECM or widely applicable.

Materials & Methods:

GelMA Synthesis and Characterization

GelMA was synthesized using a modified published protocol.[27] All materials were purchased from Sigma Aldrich (St. Louis, MO) unless otherwise specified. Porcine gelatin was dissolved at 10% w/v in reaction buffer [1.1 M sodium carbonate and 1.1M sodium bicarbonate in deionized water] at 50°C. 1% v/v Methacrylic anhydride was added dropwise and allowed to react while spinning for 3 hours at 50°C. GelMA was precipitated in acetone, then dialyzed at 50°C for 4 days. The dialyzed GelMA was then aliquoted into 50 ml conical tubes, frozen, and lyophilized. The GelMA was stored at −20°C until used.

Degree of modification was measured using TNBS assay (ThermoFisher, Waltham, MA) and confirmed using H-NMR. GelMA was compared against gelatin at 1mg/ml, and absorbance was measured at 335 nm using a Cytation3 plate reader (BioTek, Winooski, VT). For H-NMR, GelMA and gelatin samples were dissolved in deuterium oxide at 50 mg/ml and measured using Bruker Avance III HD nanobay AX-400 (Bruker, Madison, WI). Data was analyzed using TopSpin software (Bruker, Madison, WI).

Decellularization and Particle Characterization

Porcine tracheae were isolated and decellularized as previously published.[41] Porcine tissues from male Yorkshire pigs discarded from unrelated cardiac studies were provided by the University of Minnesota Visible Heart Lab. Whole tracheae were splayed with an incision along the dorsal side, and the luminal tissue was removed. Individual cartilage rings were separated from each other and cut into approximately 5mm squares.

The tissue was washed in 1x phosphate buffered saline (1xPBS). Cellular material was removed with a series of detergent, hypertonic, and enzymatic solutions: 0.1% triton x-100 (18 hours), 2% sodium deoxycholate (18 hours), 1M sodium chloride (2 hours), and 10 ug/ml DNAse in 1.3mM magnesium sulfate and 2mM calcium chloride (4 hours). The decellularized ECM was then frozen, lyophilized, and milled using a Spex Freezer/Mill 6700 (Spex, Metuchen, NJ). The dECM particles were filtered using a 100-um nylon mesh (LLL & Solutions LLC, Miami, FL).

The success of decellularization was evaluated using the Quant-iT PicoGreen DNA assay (Invitrogen, Waltham, MA) sensitive to 50 pg (Supplemental Figure 2A). Particle size was determined by imaging particles dusted in a 6 well plate using the EVOS 2 (ThermoFisher, Waltham, MA). Particle size distributions were calculated using ImageJ (Supplemental Figure 2 B & C).[42] GelMA hydrogels with and without dECM particles were prepared, frozen, sectioned at 7μm and were evaluated using standard histological stains. Masson's trichrome was used to identify collagen dense regions. Safranin-O counter stained with fast green was used to visualize glycosaminoglycan (GAG) content.

Bioink Rheological Characterization

The rheological properties of the dECM particles added to GelMA were measured using a TA Instruments DHR-3 with a lower peltier plate and an upper 40mm parallel plate attachment (TA Instruments New Castle, DE). Bulk rheological properties of GelMA-dECM mixtures were measured at 25°C and a gap of 1mm (>10X particle size). These mixtures were 5% wt/v GelMA with 0, 5, or 10% wt/v dECM particles.

Samples were conditioned for 120s at the testing temperature (15 or 25°C), then subjected to an oscillatory strain sweep from 0.01–500% at a frequency of 1.0 Hz. This strain-controlled approach allowed for all samples to be tested with the same protocol while avoiding sample ejection at high shear rates. Next, samples were conditioned for 120s at the testing temperature and subjected to an increasing shear rate sweep (range 1×10^{-2} to 1×10^{2} 1/s) to produce a flow curve. The oscillatory test characterized the viscoelastic behavior in terms of storage modulus (G') and loss modulus (G"). This allowed for the calculation of an apparent yield stress, observing the stress value at which the storage and loss moduli cross (tan(D) = 1). In cases where a yield stress could not be observed, it was inferred by fitting the flow curve data to the Herschel-Bulkley Model (Equation 1) using the TRIOS software package (TA Instruments, #4.4.0.41651, New Castle, DE).

$$\tau = \tau_o + k\dot{\gamma}^n \quad \text{(Equation 1)}$$

In this model, τ is the shear stress and $\dot{\gamma}$ is the shear rate. The parameters τ_o, k, and n are the yield stress, consistency index, and flow index, respectively. Confidence intervals for the model parameters for each ECM concentration are shown in the supplementary materials (Supplemental Table 1).

Print Resolution

To screen the effects of the dECM additive, the 2D extrusion resolution of varying concentrations was tested using cylindrical needles (20,22, and 23 gauge, ½") with constant print speed (5 mm/s), and height (0.1 mm) while the driving pressure was varied from 25 kPa to 200 kPa using a BioX bioprinter (Cellink Boston, MA). All bioinks were 5% wt/v GelMA and 1% wt/v lithium phenyl-2,4,6-trimethylbenzoylphosphinate (LAP) with 0% - 10% wt/v dECM. The subsequent fiber diameters were measured using images obtained with an EVOS 2 fluorescence imaging system (ThermoFisher, Waltham, MA).

Print Fidelity and Reproducibility

To compare the utility of dECM particles as an additive, 5% GelMA with 1% LAP printed at 15°C and 125kPa and 5% GelMA and 1% LAP with 10% dECM printed at 25°C and 75kPa were printed using the same g-code with a 18 Ga tip at 5 mm/s.

The g-code was a stack of 5 layers of rings with a 5 mm radius. The first layer height was set at 0.1 mm, and the four subsequent layers at 0.5 mm steps to 2.1 mm total height. After the prints were complete, the bottom layers were imaged using the EVOS 2. The area of the center lumen and the wall were measured using ImageJ. Circularity was calculated for the outer edge of the ring, $C = 4\pi \text{ Area/Perimeter}^2$. From this measurement, the uniformity of the ring can be compared. A perfect circle has a value of 1, and the greater the deviations from 1 the more defects are present in the printed construct. The height of these tubes was measured using the surface detection function of the MACH-1 (Biomomentum, Laval, QC, CA). Tensile testing was performed using the MACH-1 and 5mm T tensile fixtures. Rings were loaded on the tensile testing posts then pulled at 0.5 mm/s until failure. Stress and strain were calculated using established methods.[43,44]

To further explore dECM printability, a more complex geometry was tested. A pediatric scale carina was printed with 5% GelMA and 1% LAP with 10% dECM. The carina was modeled using Solidworks2020 (Solidworks Corp. Waltham, MA). The 3D model of the larynx was modified from University of Dundee and BodyParts3D, The Database Center for Life Science, "Anatomy of the Larynx" using Maya (Autodesk Inc., San Rafael, CA). The g-code was generated using Simplify3D (Simplify3D Cincinnati, Ohio) and printed using a BioX bioprinter. The printed construct was imaged using a X-TEK XT H 225 micro-CT scanner (METRIS, Leuven, Belgium). CT images were processed with CT Pro 3D (XTEK) and VGSTUDIO Max 3.2, creating DICOM files. The DICOM files were then segmented using 3D Slicer to create and export a 3D mesh.[45] The resulting 3D mesh was compared to the original model using CloudCompare (www.cloudcompare.org).

Statistical Analysis

Comparisons of means between two groups were performed by Student's T-test, and comparisons between three or more groups were performed using one-way ANOVA and Tukey's Honest Significant Difference test. Comparison of fitted Herschel-Bulkley model parameters was accomplished using confidence intervals corrected for multiple comparisons using the Bonferroni method. Where provided, error bars represent the standard deviation.

All statistical tests were performed using JMP 15.1.0. Graphs were created using Prism, JMP 15.1.0 or Microsoft Excel.

Supplementary Material

Refer to Web version on PubMed Central for supplementary material.

Acknowledgements

The authors would like to acknowledge the Visible Heart Lab for porcine tissue donation, the UMN Polymer Characterization Facility, the Minnesota Dental Research Center for Biomaterials and Biomechanics, and the UMN 3D Bioprinting Facility. This work was supported by the National Institutes of Health NHLBI F31 (5F31HL142313) awarded to Z. P. Galliger, a CTSI Translational Research Development Program grant awarded to Z. P. Galliger (from the National Center for Advancing Translational Sciences grant UL1TR002494. PI: B. Blazar. The content is solely the responsibility of the authors and does not necessarily represent the official views of the National Institutes of Health's National Center for Advancing Translational Sciences.), the T32 (5T32HL007741) training grant for C. D. Vogt (Training in Pulmonary Science, PI: D. Ingbar), and non-sponsored funds (A. Panoskaltsis-Mortari).

References:

1. Benton JA, DeForest CA, Vivekanandan V, Anseth KS. Photocrosslinking of gelatin macromers to synthesize porous hydrogels that promote valvular interstitial cell function. Tissue Eng Part A. 2009;15(11):3221–3230. doi:10.1089/ten.TEA.2008.0545 [PubMed: 19374488]
2. Kupfer ME, Lin WH, Ravikumar V, et al. In Situ Expansion, Differentiation and Electromechanical Coupling of Human Cardiac Muscle in a 3D Bioprinted, Chambered Organoid. Circulation Research. Published online 2020:207–224. doi:10.1161/circresaha.119.316155 [PubMed: 32228120]
3. Abbadessa A, Mouser VHM, Blokzijl MM, et al. A Synthetic Thermosensitive Hydrogel for Cartilage Bioprinting and Its Biofunctionalization with Polysaccharides. Biomacromolecules. 2016;17(6):2137–2147. doi:10.1021/acs.biomac.6b00366 [PubMed: 27171342]
4. Hinton TJ, Jallerat Q, Palchesko RN, et al. Three-dimensional printing of complex biological structures by freeform reversible embedding of suspended hydrogels. Science Advances. 2015;1(9). doi:10.1126/sciadv.1500758
5. Price AP, England KA, Matson AM, Blazar BR, Panoskaltsis-Mortari A. Development of a Decellularized Lung Bioreactor System for Bioengineering the Lung: The Matrix Reloaded. Tissue Engineering Part A. 2010;16(8):2581–2591. doi:10.1089/ten.tea.2009.0659 [PubMed: 20297903]
6. Sun Y, Yan L, Chen S, Pei M. Functionality of decellularized matrix in cartilage regeneration: A comparison of tissue versus cell sources. Acta Biomaterialia. 2018;74:56–73. doi:10.1016/j.actbio.2018.04.048 [PubMed: 29702288]
7. Xu Y, Li D, Yin Z, et al. Tissue-engineered trachea regeneration using decellularized trachea matrix treated with laser micropore technique. Acta Biomaterialia. 2017;58:113–121. doi:10.1016/j.actbio.2017.05.010 [PubMed: 28546133]
8. Ansari T, Lange P, Southgate A, et al. Stem Cell-Based Tissue-Engineered Laryngeal Replacement. Stem Cells Translational Medicine. 2017;6(2):677–687. doi:10.5966/sctm.2016-0130 [PubMed: 28191770]
9. Abaci A, Guvendiren M. Designing Decellularized Extracellular Matrix-Based Bioinks for 3D Bioprinting. Advanced Healthcare Materials. 2020;2000734:1–18. doi:10.1002/adhm.202000734
10. De Santis MM, Alsafadi HN, Tas S, et al. Extracellular-Matrix-Reinforced Bioinks for 3D Bioprinting Human Tissue. Advanced Materials. 2021;33(3). doi:10.1002/adma.202005476
11. Pouliot RA, Young BM, Link PA, et al. Porcine Lung-Derived Extracellular Matrix Hydrogel Properties Are Dependent on Pepsin Digestion Time. Tissue Engineering - Part C: Methods. 2020;26(6):332–346. doi:10.1089/ten.tec.2020.0042 [PubMed: 32390520]

12. Ma X, Yu C, Wang P, et al. Rapid 3D bioprinting of decellularized extracellular matrix with regionally varied mechanical properties and biomimetic microarchitecture. Biomaterials. 2018;185:310–321. doi:10.1016/j.biomaterials.2018.09.026 [PubMed: 30265900]

13. Lin H, Yang G, Tan J, Tuan RS. Influence of decellularized matrix derived from human mesenchymal stem cells on their proliferation, migration and multi-lineage differentiation potential. Biomaterials. 2012;33(18):4480–4489. doi:10.1016/j.biomaterials.2012.03.012 [PubMed: 22459197]

14. Schwarz S, Koerber L, Elsaesser AF, et al. Decellularized Cartilage Matrix as a Novel Biomatrix for Cartilage Tissue-Engineering Applications. Tissue Engineering Part A. 2012;18:120720085805006. doi:10.1089/ten.tea.2011.0705

15. Dequach JA, Yuan SH, Goldstein LSB, Christman KL. Decellularized porcine brain matrix for cell culture and tissue engineering scaffolds. Tissue Engineering - Part A. 2011;17(21–22):2583–2592. doi:10.1089/ten.tea.2010.0724 [PubMed: 21883047]

16. Freytes DO, Martin J, Velankar SS, Lee AS, Badylak SF. Preparation and rheological characterization of a gel form of the porcine urinary bladder matrix. Biomaterials. 2008;29(11):1630–1637. doi:10.1016/j.biomaterials.2007.12.014 [PubMed: 18201760]

17. Kusuma GD, Yang MC, Brennecke SP, O'Connor AJ, Kalionis B, Heath DE. Transferable Matrixes Produced from Decellularized Extracellular Matrix Promote Proliferation and Osteogenic Differentiation of Mesenchymal Stem Cells and Facilitate Scale-Up. ACS Biomaterials Science and Engineering. 2018;4(5):1760–1769. doi:10.1021/acsbiomaterials.7b00747 [PubMed: 33445333]

18. Poon CJ, Maria M v., Sinha S, et al. Preparation of an adipogenic hydrogel from subcutaneous adipose tissue. Acta Biomaterialia. 2013;9(3):5609–5620. doi:10.1016/j.actbio.2012.11.003 [PubMed: 23142702]

19. Wolf MT, Daly KA, Brennan-Pierce EP, et al. A hydrogel derived from decellularized dermal extracellular matrix. Biomaterials. 2012;33(29):7028–7038. doi:10.1016/j.biomaterials.2012.06.051 [PubMed: 22789723]

20. Visser J, Levett PA, te Moller NCR, et al. Crosslinkable hydrogels derived from cartilage, meniscus, and tendon tissue. Tissue Eng Part A. 2015;21(7–8):1195–1206. doi:10.1089/ten.TEA.2014.0362 [PubMed: 25557049]

21. Beck EC, Barragan M, Tadros MH, Gehrke SH, Detamore MS. Approaching the compressive modulus of articular cartilage with a decellularized cartilage-based hydrogel. Acta Biomaterialia. 2016;38(785):94–105. doi:10.1016/j.actbio.2016.04.019 [PubMed: 27090590]

22. Beck EC, Barragan M, Libeer TB, et al. Chondroinduction from Naturally Derived Cartilage Matrix: A Comparison Between Devitalized and Decellularized Cartilage Encapsulated in Hydrogel Pastes. Tissue Engineering - Part A. 2016;22(7–8):665–679. doi:10.1089/ten.tea.2015.0546 [PubMed: 27001140]

23. Visser J, Gawlitta D, Benders KEM, et al. Endochondral bone formation in gelatin methacrylamide hydrogel with embedded cartilage-derived matrix particles. Biomaterials. 2015;37:174–182. doi:10.1016/j.biomaterials.2014.10.020 [PubMed: 25453948]

24. Krüger T Computer Simulation Study of Collective Phenomena in Dense Suspensions of Red Blood Cells under Shear. Vieweg+Teubner Verlag; 2012. doi:10.1007/978-3-8348-2376-2

25. Bentz DP, Ferraris CF, Galler MA, Hansen AS, Guynn JM. Influence of particle size distributions on yield stress and viscosity of cement-fly ash pastes. Cement and Concrete Research. 2012;42(2):404–409. doi:10.1016/j.cemconres.2011.11.006

26. Skylar-Scott MA, Uzel SGM, Nam LL, et al. Biomanufacturing of organ-specific tissues with high cellular density and embedded vascular channels. Science Advances. 2019;5(9). doi:10.1126/sciadv.aaw2459

27. Shirahama H, Lee BH, Tan LP, Cho NJ. Precise Tuning of Facile One-Pot Gelatin Methacryloyl (GelMA) Synthesis. Sci Rep. 2016;6(August):31036. doi:10.1038/srep31036 [PubMed: 27503340]

28. Loessner D, Meinert C, Kaemmerer E, et al. Functionalization, preparation and use of cell-laden gelatin methacryloyl-based hydrogels as modular tissue culture platforms. Nature Protocols. 2016;11(4):727–746. doi:10.1038/nprot.2016.037 [PubMed: 26985572]

29. Yue K, Li X, Schrobback K, et al. Structural analysis of photocrosslinkable methacryloyl-modified protein derivatives. Biomaterials. 2017;139:163–171. doi:10.1016/j.biomaterials.2017.04.050 [PubMed: 28618346]
30. Zhang Z, Jin Y, Yin J, et al. Evaluation of bioink printability for bioprinting applications. Applied Physics Reviews. 2018;5(4). doi:10.1063/1.5053979
31. Lee A, Hudson AR, Shiwarski DJ, et al. 3D bioprinting of collagen to rebuild components of the human heart. Science (1979). 2019;365(6452):482–487. doi:10.1126/science.aav9051
32. Hinton TJ, Lee A, Feinberg AW. 3D bioprinting from the micrometer to millimeter length scales: Size does matter. Current Opinion in Biomedical Engineering. 2017;1:31–37. doi:10.1016/j.cobme.2017.02.004
33. Mahzoon S, Detamore MS. Chondroinductive Peptides: Drawing Inspirtations from Cell-Matrix Interactions. 2019;25(3):249–257. doi:10.1089/ten.teb.2018.0003
34. Kim YS, Majid M, Melchiorri AJ, Mikos AG. Applications of decellularized extracellular matrix in bone and cartilage tissue engineering. Bioengineering & Translational Medicine. 2019;4(1):83–95. doi:10.1002/btm2.10110 [PubMed: 30680321]
35. Sun Y, Yan L, Chen S, Pei M. Functionality of decellularized matrix in cartilage regeneration: A comparison of tissue versus cell sources. Acta Biomaterialia. 2018;74:56–73. doi:10.1016/j.actbio.2018.04.048 [PubMed: 29702288]
36. Rothrauff BB, Shimomura K, Gottardi R, Alexander PG, Tuan RS. Anatomical region-dependent enhancement of 3-dimensional chondrogenic differentiation of human mesenchymal stem cells by soluble meniscus extracellular matrix. Acta Biomaterialia. 2017;49:140–151. doi:10.1016/j.actbio.2016.11.046 [PubMed: 27876676]
37. Utomo L, Pleumeekers MM, Nimeskern L, et al. Preparation and characterization of a decellularized cartilage scaffold for ear cartilage reconstruction. Biomedical Materials (Bristol). 2015;10(1). doi:10.1088/1748-6041/10/1/015010
38. Chang CH, Chen CC, Liao CH, Lin FH, Hsu YM, Fang HW. Human acellular cartilage matrix powders as a biological scaffold for cartilage tissue engineering with synovium-derived mesenchymal stem cells. Journal of Biomedical Materials Research - Part A. 2014;102(7):2248–2257. doi:10.1002/jbm.a.34897 [PubMed: 23913750]
39. Neill T, Schaefer L, Iozzo RV. Decoding the Matrix: Instructive Roles of Proteoglycan Receptors. Biochemistry. 2015;54(30):4583–4598. doi:10.1021/acs.biochem.5b00653 [PubMed: 26177309]
40. Zha K, Sun Z, Yang Y, et al. Recent developed strategies for enhancing chondrogenic differentiation of MSC: Impact on MSC-based therapy for cartilage regeneration. Stem Cells International. 2021;2021. doi:10.1155/2021/8830834
41. Galliger Z, Panoskaltsis-Mortari A. Tracheal Cartilage Isolation and Decellularization. In: Humana Press; 2017:155–160. doi:10.1007/7651_2017_52
42. Schindelin J, Arganda-Carreras I, Frise E, et al. Fiji: An open-source platform for biological-image analysis. Nature Methods. 2012;9(7):676–682. doi:10.1038/nmeth.2019 [PubMed: 22743772]
43. Lillie MA, Chalmers GWG, Gosline JM. The effects of heating on the mechanical properties of arterial elastin. Connective Tissue Research. 1994;31(1):23–35. doi:10.3109/03008209409005632 [PubMed: 15609619]
44. Lillie MA, Gosline JM. Mechanical properties of elastin along the thoracic aorta in the pig. Journal of Biomechanics. 2007;40(10):2214–2221. doi:10.1016/j.jbiomech.2006.10.025 [PubMed: 17174959]
45. Fedorov A, Beichel R, Kalpathy-Cramer J, et al. 3D Slicer as an image computing platform for the Quantitative Imaging Network. Magnetic Resonance Imaging. 2012;30(9):1323–1341. doi:10.1016/j.mri.2012.05.001 [PubMed: 22770690]

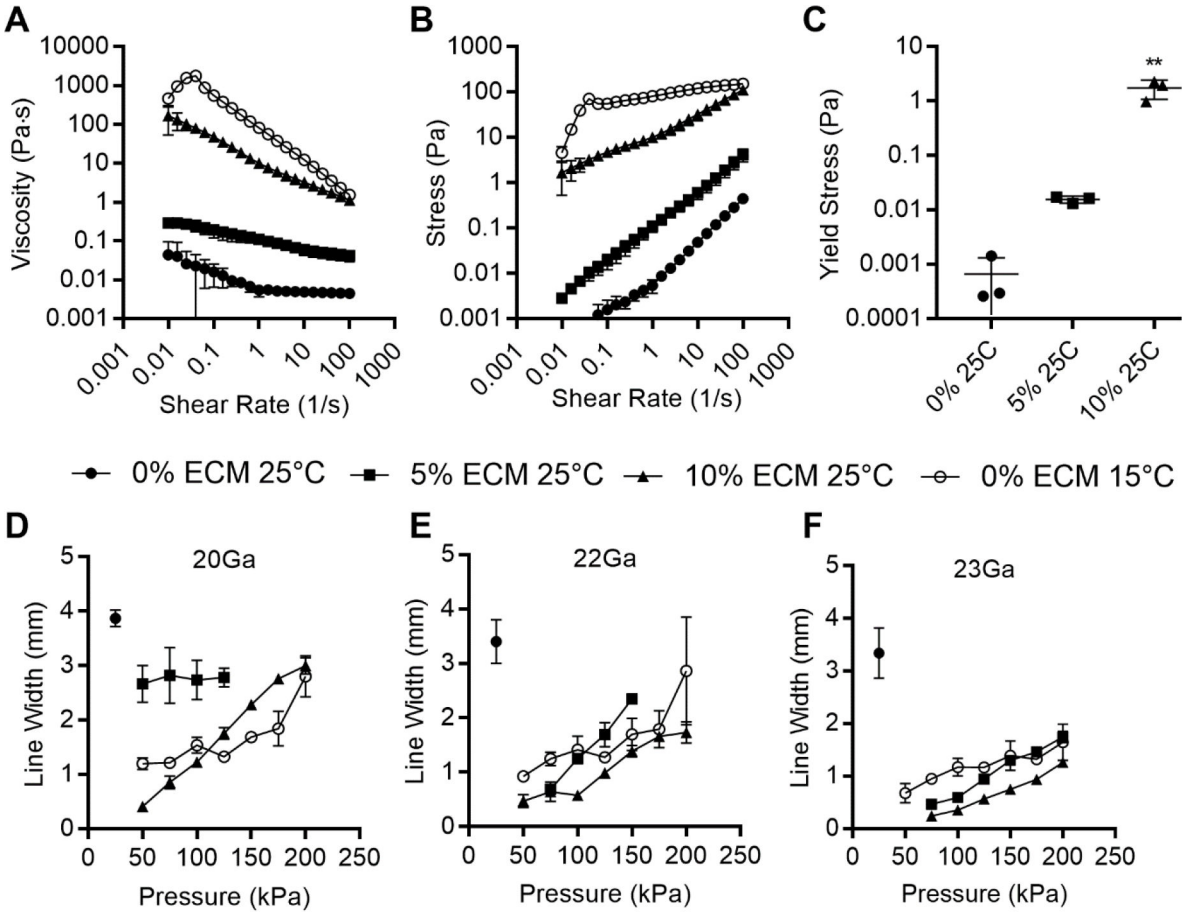

Figure 1:

dECM dose dependent rheology. 10% GelMA with dECM ranging from 0%–20% wt/v: A) Shear rate flow sweep, n = 3. B) Mean thixotropic hysteresis loops. C) Apparent yield stress, n =3, [**p<.01] between groups. D-F) Plot of filament thickness versus pressure for each bioink through 20Ga, 22Ga or 23Ga needles respectively, plotted as mean ± standard deviation n = 3, significance not shown for clarity, values shown in Supplemental Table 1.

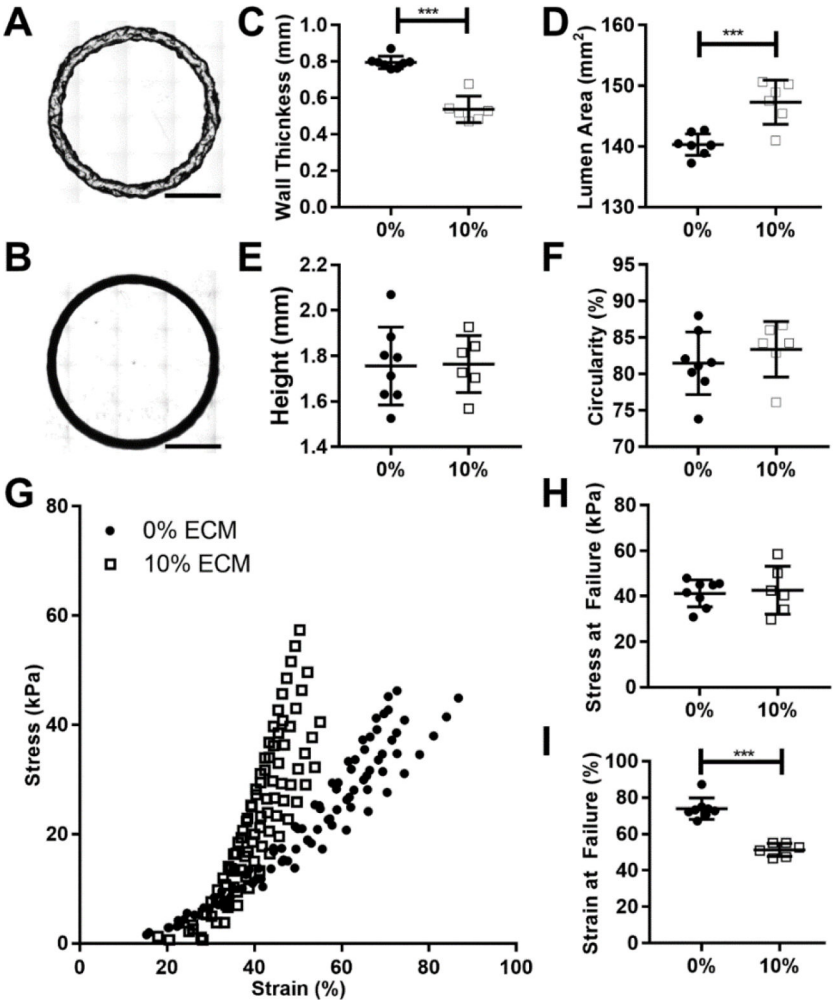

Figure 2:

Print fidelity and reproducibility of simple geometries. A) Representative image of 5% wt/v GelMA ring printed at 15°C, scale bar 5mm. B) Representative image of 5% wt/v GelMA with 10% wt/v dECM ring printed at 25°C, scale bar 5mm. C) Graph of ring wall thickness (mm). D) Graph of lumen area (mm^2). E) Graph of ring heights (mm). F) Graph of ring outer edge circularity (%). G) Graph of tensile failure, individual runs plotted, 0% at 15°C n= 8, 20% at 25°C n = 6. H) Stress at failure for each construct. I) Strain at failure for each construct. [p<.05 *, p<.01 **, p<.001 ***]

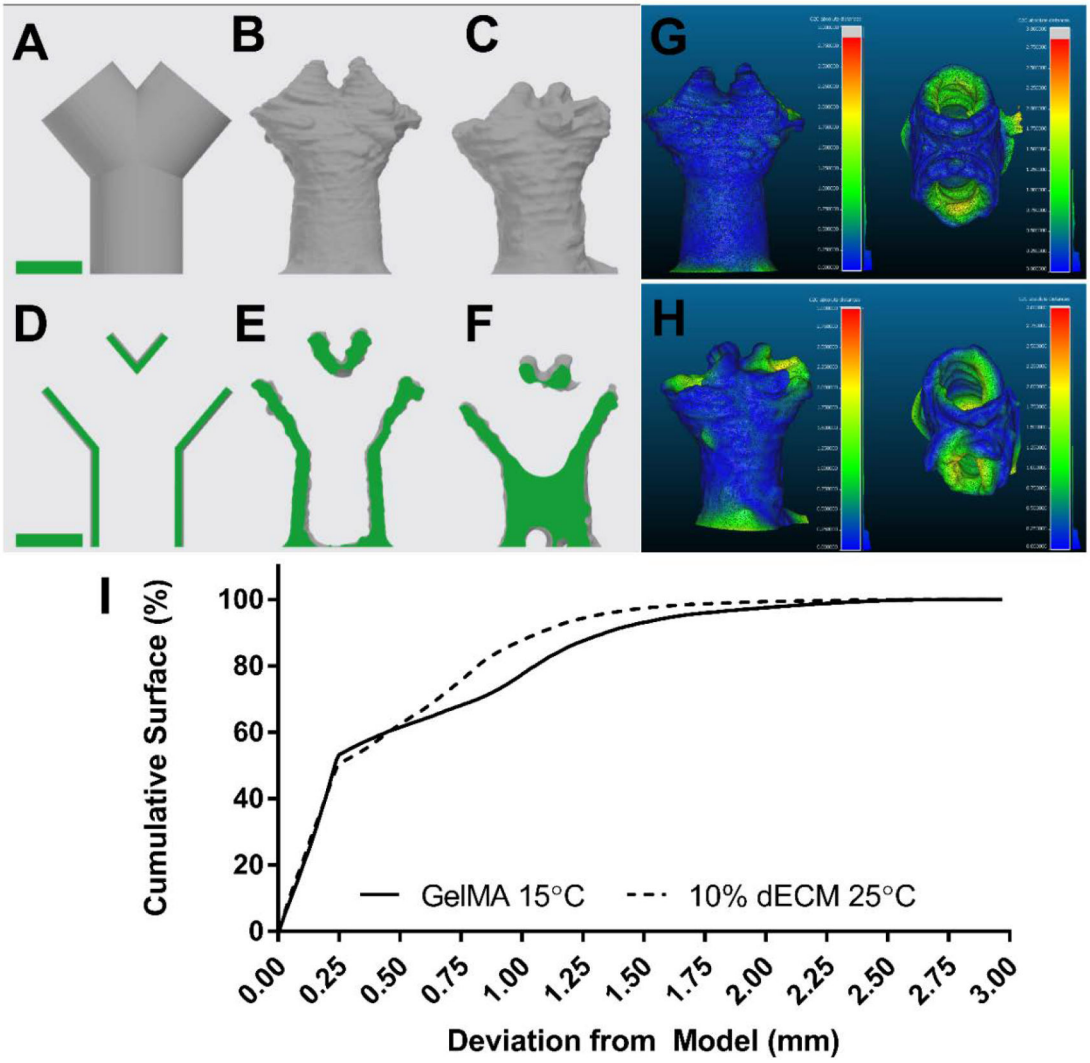

Figure 3:

Fidelity of self-supporting carina. A&D) Carina model geometry, B&E) 3D reconstruction of dECM printed carina, C&F) reconstruction of GelMA printed carina, full surface scale bars 5mm. G) computed distance between dECM printed carina and model geometry, side (left) and top (right) view. H) computed distance between GelMA printed carina and model geometry, side (left) and top (right). I) Cumulative surface distances between bioprinted constructs and model geometry.

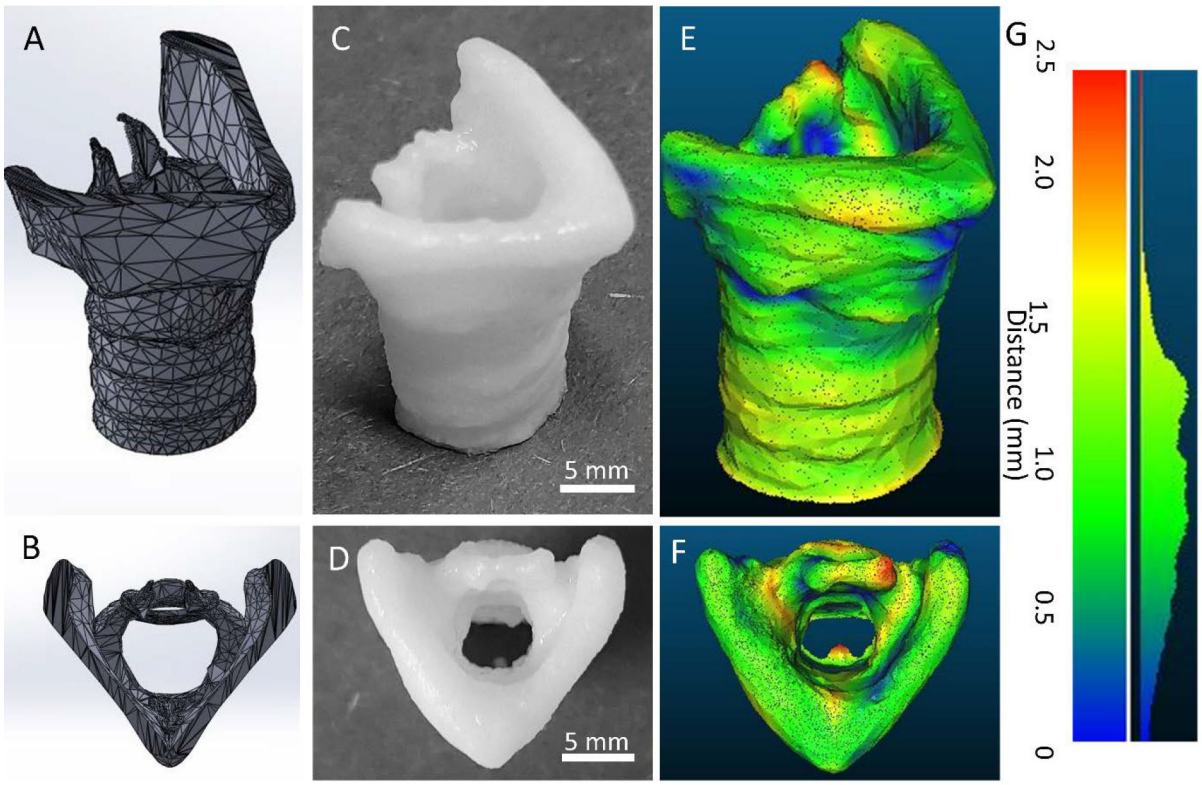

Figure 4:

Fidelity of self-supporting, ECM bioink larynx. A & B) Larynx digital model geometry, side and top view respectively. C & D) ECM particle-laden bioprinted larynx construct side and top view respectively, 5 mm scale bar. E & F) Surface map of distance between digital model geometry and bioprinted larynx, side and top view respectively. G) histogram of the distances is shown on the right.

Table 1:

Herschel-Bulkley Model Parameters. 95% Confidence Intervals (Bonferroni corrected) for Parameters of Herschel-Bulkley Model fit.

ECM Concentration	τ_o		k		n	
0%	0.01	−0.01	0.01	0.01	1.04	0.88
5%	9.98	−5.31	14.33	−5.18	0.48	0.30
10%	5.40	−0.73	8.42	0.73	0.58	0.20
15%	12.22	−3.07	33.61	14.10	0.44	0.26
20%	28.11	−13.95	133.65	79.93	0.35	0.25